KSCE Journal of Civil Engineering (0000) 00(0):1-11
DOI 10.1007/s12205-017-1535-4

Geotechnical Engineering
pISSN 1226-7988, eISSN 1976-3808
www.springer.com/12205

Boundary Effect on the Seismic Response of a Three-dimensional Soil Slope with a Shallow Foundation on Top

Shengyi Cong*, Liang Tang, Xianzhang Ling***, Lin Geng****, and Jinchi Lu*****

Received September 4, 2016/Revised February 26, 2017/Accepted April 12, 2017/Published Online June 23, 2017

Abstract

Numerical approaches are providing a versatile environment for conducting the studies of slopes and shallow foundations on the top of slopes. However, there are few studies for assessing the boundary effects on the seismic response of a soil slope and the dynamic behaviors of a shallow foundation on top of three-dimensional (3D) slopes. On the basis of a systematic parametric study, Finite Element (FE) simulations are firstly conducted to evaluate the boundary effect on the seismic performance of the soil slope. Then, the boundary effects on the behaviors of a shallow foundation on top of a 3D slope under the earthquake loadings are addressed. The results show that for a given 3D soil slope, fixing the displacement degrees of freedom only in the y-direction (perpendicular to the shaking direction) at the lateral boundaries is inappropriate, because this approach does not consider the 3D effect. A smaller slope's width/height ratio is obtained for stiffer soil, compared to soft soil, as the 3D effects induced by the lateral boundaries lose significance. The earthquake characteristics (peak ground accelerations and frequency content) play important roles in the differences among the three lateral boundaries. Furthermore, when the boundary extent along the y-direction is increased, the foundation settlement that is controlled by the applied pressure and earthquake loading together, will be mostly affected by the seismic excitation. Overall, the conducted study highlights the significance of boundary conditions on the seismic responses of soil slopes and a shallow foundation on the top of it and can be helpful for engineers to choose an appropriate boundary in numerical analysis.

Keywords: *boundary effect, seismic response, numerical analysis, soil slope, shallow foundation*

1. Introduction

Seismic failure of slopes and geotechnical structures (e.g., shallow foundations, retaining walls, bored piles, sheet pile walls, tunnel cut-and-cover walls, tunnel linings) has been a major cause of human and material losses and has also been the subject of much research (Bouckovalas and Papadimitriou, 2005; Azizian and Popescu, 2006; Kourkoulis *et al*., 2010; Taiebat *et al*., 2011; Tripe *et al*., 2013; Azzam, 2015; Karimi and Dashti, 2015; Liu *et al*., 2015). In some cases, geotechnical structures are constructed adjacent to an earth dike or sloping surface such as footings for bridge abutments near river dikes on sloping embankments (Kourkoulis *et al*., 2010; Azzam, 2015). Excessive permanent deformation of shallow foundations on top of slopes under earthquake loading has been widely observed (Choudhury and Subba, 2006; Kourkoulis *et al*., 2010; Azzam, 2015).

Numerous experimental studies on the seismic behavior of a shallow foundation on a level ground have been performed, including shake-table experiments (Maugeri *et al*., 2000; Paolucci *et al*., 2008; Shirato *et al*., 2008; Drosos *et al*., 2012; Karimi and Dashti, 2015) and centrifuge tests (Gajan *et al*., 2005; Bienen *et al*., 2007; Gajan and Kutter, 2009; Raychowdhury and Hutchinson, 2009; Deng and Kutter, 2012; Trombetta *et al*., 2013). Up to now, very few studies have been conducted on the dynamic behavior of a shallow foundation on top of a slope. Compared to a physical experiment, the Finite Element (FE) method is a less expensive and less time-consuming way, and offers the advantage of conveniently simulating more influencing factors. In this environment, a number of seismic behaviors of shallow foundations resting on top of slopes have been adequately analyzed via the FE method (Choudhury and Subba, 2006; Kourkoulis *et al*., 2010; Azzam, 2015). The seismic response problems in geotechnical earthquake engineering practices involve boundary values. Therefore, boundary conditions can play an important role in the development of internal stresses on the soil slope and can affect the seismic bearing capacity of the shallow foundation. Literatures about the boundary effects on the dynamic characteristics of a soil slope as well as a shallow foundation founded near 3D slope

*Ph.D. Student, School of Civil Engineering, Harbin Institute of Technology, Harbin, China (E-mail: csy_hit@163.com)
**Professor, School of Civil Engineering, Harbin Institute of Technology, Harbin, China (Corresponding Author, E-mail: hit_tl@163.com)
***Professor, School of Civil Engineering, Harbin Institute of Technology, Harbin, China (E-mail: xianzhang_ling@263.net)
****Ph.D. Student, School of Civil Engineering, Harbin Institute of Technology, Harbin, China (E-mail: gl_hit@163.com)
*****Associate Project Scientist, Dept. of Structural Engineering, University of California, San Diego, USA (E-mail: jinlu@ucsd.edu)

crests are few.

In the following sections, the numerical framework for simulating the seismic response of a 3D soil slope and the dynamic settlement of a shallow foundation on top of the slope are described. Emphasis is placed on the boundary effect on the seismic slope response, and then the boundary effect on the seismic settlement of the shallow foundation is discussed. Finally, insights and conclusions are drawn based on the reported results.

2. Numerical Modeling of Soil Slope

All simulations were conducted using the open-source computational platform OpenSees (http://opensees.berkeley.edu, Mazzoni *et al*., 2006). This platform allows for developing applications to simulate the performance of structural and geotechnical systems subjected to static and seismic loadings.

2.1 Finite Element Mesh

Three representative types of soil slopes named as Types 1, 2 and 3 that are common in practical engineering are employed as shown in Fig. 1. The profile consists of a 15-m-thick foundation soil overlain by a 15 m high slope (H = 15 m) with slope angles (α) of 15º, 25º, and 35º. Type 1 is a homogeneous soil slope. Type 2 includes a 9-m-thick stiff clay layer in the lower portion and a 21-m-thick medium clay layer in the upper portion. In Type 3, three layers consisting of medium clay (18-m in thickness), soft clay (3-m in thickness), and stiff clay (9-m in thickness) are considered (from bottom up, see Fig. 1).

A homogeneous soil slope with a slope angle of 25º is used to show the FE meshes (Fig. 2). The soil slope with a length of 142 m and a slope angle of 25º is considered to lie in the xz plane [Fig. 2(a)], and the width of the slope is 100 m (W = 100 m) in the y-direction [Fig. 2(b)]. Every node in the 3D model including the boundaries has three degrees of freedom, i.e. displacements

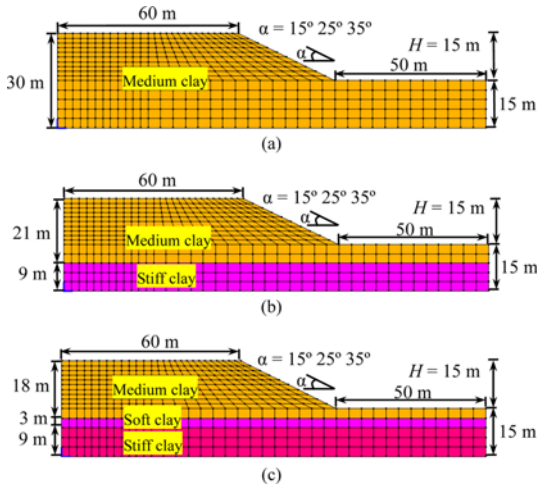

Fig. 1. Three Representative Types of Soil Slopes: (a) a Homogeneous Soil Slope (Type 1), (b) a Stratified Soil Slope (Type 2), (c) a Soil Slope with a Soft Clay Interlayer (Type 3) for Example calculations

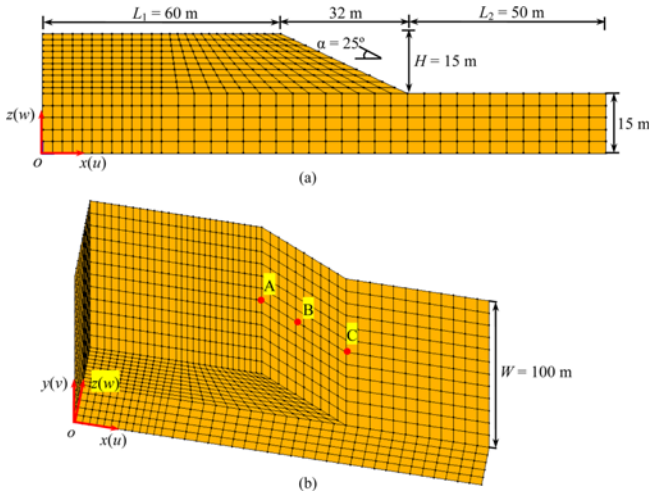

Fig. 2. Model Geometry and Finite Element Meshes: (a) 2D Mesh, (b) 3D mesh (Mesh 1)

u, v and w in the x-, y- and z-directions, respectively [Fig. 2(b)]. Nodes A, B, and C, depicted by solid circles in Fig. 2(b) and located on the plane of symmetry (i.e., y = 50 m), are at elevations of 30, 24 m, and 15 m from the base. For the 3D analyses, the soil domain is discretized with 8-node brick elements, which are hexahedral linear isoparametric elements.

2.2 Constitutive Modeling of Soil

Clay material is modeled as a nonlinear hysteretic material (Parra, 1996; Lu *et al*., 2010; Yang *et al*., 2003) with a Von Mises multi-surface (Iwan, 1967; Mroz, 1967) kinematic plasticity model. The hyperbolic backbone curve can be approximated by the hyperbolic formula (Yang *et al*., 2003):

$$\tau = G_r\gamma / \left(1+\gamma / \gamma_r\right) \tag{1}$$

where G_r = Low-strain shear modulus (Fig. 3)

γ_r = τ_{max}/G_r in which τ_{max} is the maximum shear strength when γ approaches ∞

τ and γ = Octahedral shear stress and strain, respectively

In order to reach the maximum shear strength at finite strain, the hyperbolic curve is often capped at $\tau_f < \tau_{max}$ (Fig. 3).

With the framework of multi-surface plasticity, the hyperbolic

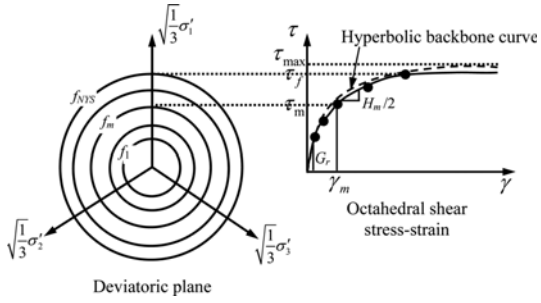

Fig. 3. Hyperbolic Backbone Curve for Soil Nonlinear Shear Stress–strain Response and Piecewise-linear Representation in Multi-yield-surface Plasticity (Yang *et al*., 2003)

Table 1. Clay Material Properties (Lu *et al.*, 2010)

Parameters	Soft clay	Medium clay	Stiff clay
Mass density (kg/m^3)	1300	1500	1800
Shear modulus (MPa)	13	60	150
Bulk modulus (MPa)	65	300	750
Cohesion (kPa)	18	37	75
Peak shear strain	0.1	0.1	0.1

backbone [Eq. (1)] is replaced by a piecewise linear approximation (Fig. 3). Each linear segment (Fig. 3) represents the domain of a yield surface f_m, characterized by elastoplastic (tangent) shear modulus H_m and size M_m, for m = 1, 2, …, NYS, where NYS is the total number of yield surfaces (The number of yield surfaces used for the clays is 20). H_m is conveniently defined by (Fig. 3):

$$H_m = 2\left(\tau_{m+1} - \tau_m\right) / \left(\gamma_{m+1} - \gamma_m\right) \tag{2}$$

with $H_{NYS} = 0$. The size of surface f_m is now dictated by (Fig. 3):

$$M_m = 3\tau_m / \sqrt{2}\left(P_r' + P_0'\right) \tag{3}$$

With $M_{NYS} = M_f$ and $\tau_{NYS} = \tau_f$.

Based on elasticity theory, the bulk modulus of the soil skeleton, B, is defined by $B = 3G(1 + \eta)/(3–6\eta)$, where η is the Poisson ratio. Furthermore, the material properties used in this study are listed in Table 1, as reported in Lu *et al.* (2010).

2.3 Boundary Conditions and Earthquake Loading

All nodes at the lateral faces (i.e., $y = 0$ and $y = 100$ faces) are constrained by displacement degrees of freedom in the (y, z) directions (i.e., $v = w = 0$ at the lateral faces). Additionally, the transmitting boundary is employed to deal with the front and back faces (i.e., $x = 142$ and $x = 0$ faces) along the shaking direction, which ensure insignificant contamination of the response with wave reflections. In addition, front and back faces are at a distance of 50 m and 60 m from the area of interest (near the slope), respectively, which can avoid significant contamination with wave reflections. The nodes at the base ($z = 0$ face) are fully fixed in all directions under application of own weight, and the displacement degrees of freedom along the shaking direction are free until the earthquake acceleration is applied at the model base. In terms of base excitation, a series of realistic earthquake motions (Fig. 4) are consecutively applied to the base of the model in each analysis. The characteristics of these earthquake motions are listed in Table 2.

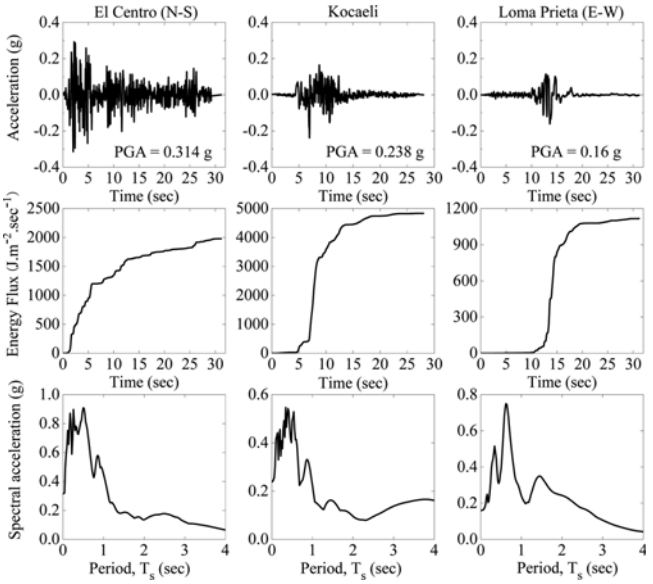

Fig. 4. Horizontal Acceleration Time History, Earthquake Energy, and 5%-damped Spectral Acceleration of the Input Events

3. Boundary Effect on the Seismic Response of Soil Slope

3.1 Influence of the Boundary Conditions at the Lateral Faces

Three types of boundary conditions at the lateral faces are used in FE analysis: (1) Case 1: fixing the y-direction displacement ($v = 0$), which represents contact with a rigid, smooth abutment providing a reacting thrust but without in-plane shear restraint; (2) Case 2: fixing the x- and y-direction displacement ($u = v = 0$); and (3) Case 3: fixing the y- and z-direction displacement ($v = w = 0$). Cases 2 and 3 represent a contact that provides side shear resistance.

Figures 5-7 show the horizontal displacement time histories at

Table 2. Earthquake Data for Analysis

Earthquake motion parameters	El Centro (USA)/N-S	Kocaeli (Turkey)	Loma Prieta (USA)/E-W
Date of occurrence	18/05/1940	08/17/1999	18/10/1989
Recording station	117 El Centro	Treasure Island	Gebze
Moment magnitude of earthquake, M_w	7.1	7.4	6.9
Maximum horizontal acceleration, MHA (g)	0.314	0.238	0.16
Predominant period, T_p (sec)	0.5	0.34	0.62
Bracketed duration (sec)	28.78	20.39	17.76
Significant duration, $D_{5\text{-}95}$ (sec)	23.84	7.49	4.4
PGV/PGA (sec)	0.116	0.223	0.21
Arias intensity (m/sec)	1.69	0.533	0.36
Energy flux (J m^{-2} sec^{-1})	1977	4835	1117
Number of significant excitation cycles, N_c	14.5	6.5	5.8

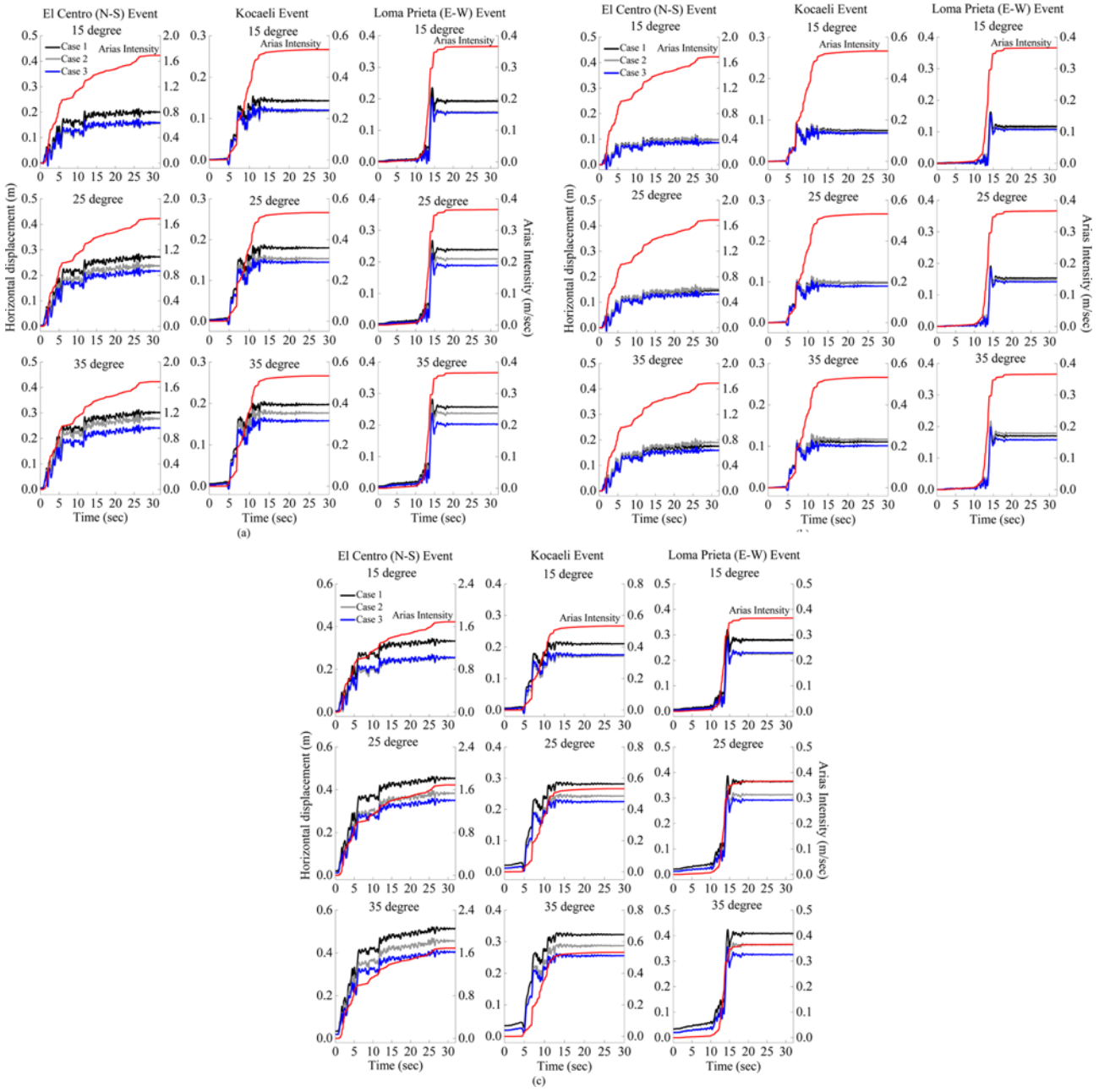

Fig. 5. Horizontal Displacement Time Histories at Node A for 3 Input Motions for: (a) Homogeneous Soil Slope, (b) Stratified Soil Slope, (c) Soil Slope with a Soft Clay Interlayer for α = 15º, 25º and 35º

Node A, the horizontal displacement color contours at the end of the seismic shaking, and 5%-damped spectral accelerations at Node A under the three types of boundaries at the lateral faces. Fig. 8 presents the effects of peak ground accelerations (PGA) on the three types of lateral boundaries. The natural frequencies of Cases 1-3 for the three types of soil slopes with a slope angle (α) of 25º are shown in Tables 3-5.

When α = 15º, the horizontal displacement at Node A in Case 2 is quite similar to the horizontal displacement in Case 3 (Fig. 5). As the slope angle becomes significant (α = 25º and 35º), the difference in the horizontal displacements at Node A between Case 2 and Case 3 increases. This is true for all the three types of soil slopes. Moreover, the horizontal displacement in Case 1 is larger than the horizontal displacement in Cases 2 and 3, except for type 2 (Fig. 5). In type 2, no significant difference in displacements between Case 1 and Case 2 is found. The natural frequencies of Case 1 and Case 2 for type 2 with a slope angle of 25º are quite similar in amplitude (Table 4). Furthermore, the influence of lateral boundaries on the natural frequency of stiffer soil stratum is not significant. Therefore, as the soil stiffness increases (types 1 and 2), comparing to the type 3 of soil slope, the natural frequency of soil slope is increased and the difference

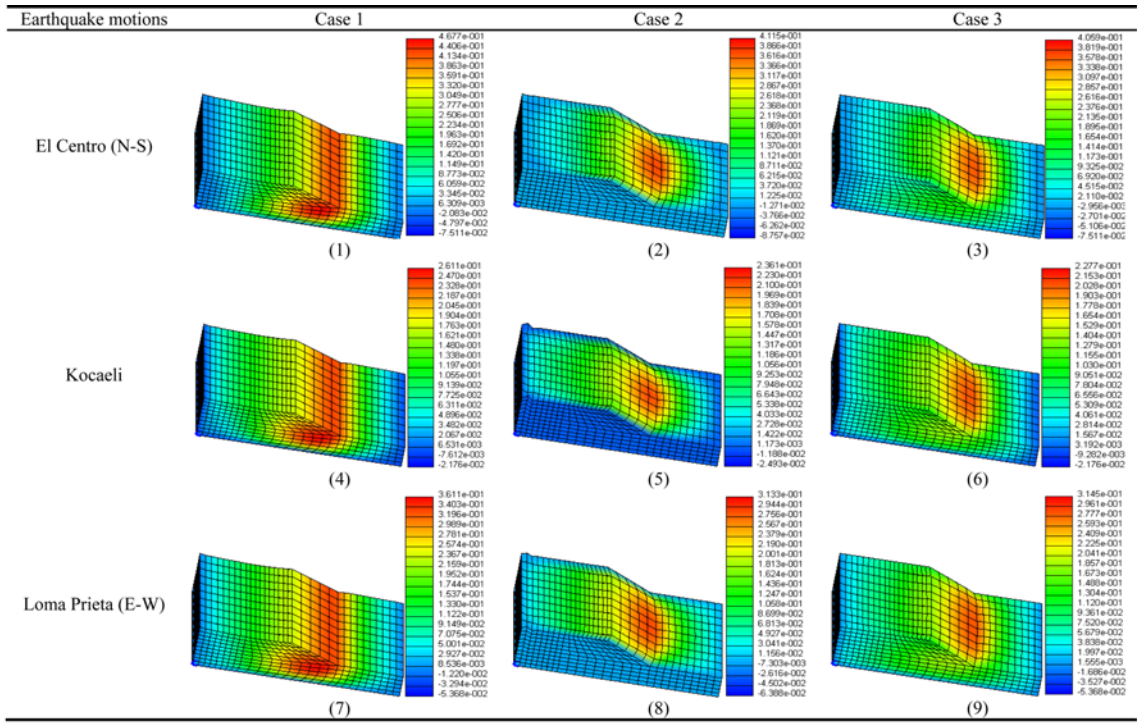

Fig. 6. Horizontal Displacement Contours for 3 Input Motions for: (a) Homogeneous Soil Slope, (b) Stratified Soil Slope, (c) Soil Slope with a Soft Clay Interlayer for α = 25º

of natural frequency for the three lateral boundaries is not significant (Tables 3 and 4).

As seen from Fig. 6, a distinct 2D shape of the deformation pattern in Case 1 and a 3D deformation pattern in Cases 2 and 3 are observed for the three types of soil slopes for the three earthquake motions. The spectral accelerations at Node A, considering a damping ratio of 5%, in Case 1 become nearly identical to the spectral accelerations at Node A in Case 3 for all

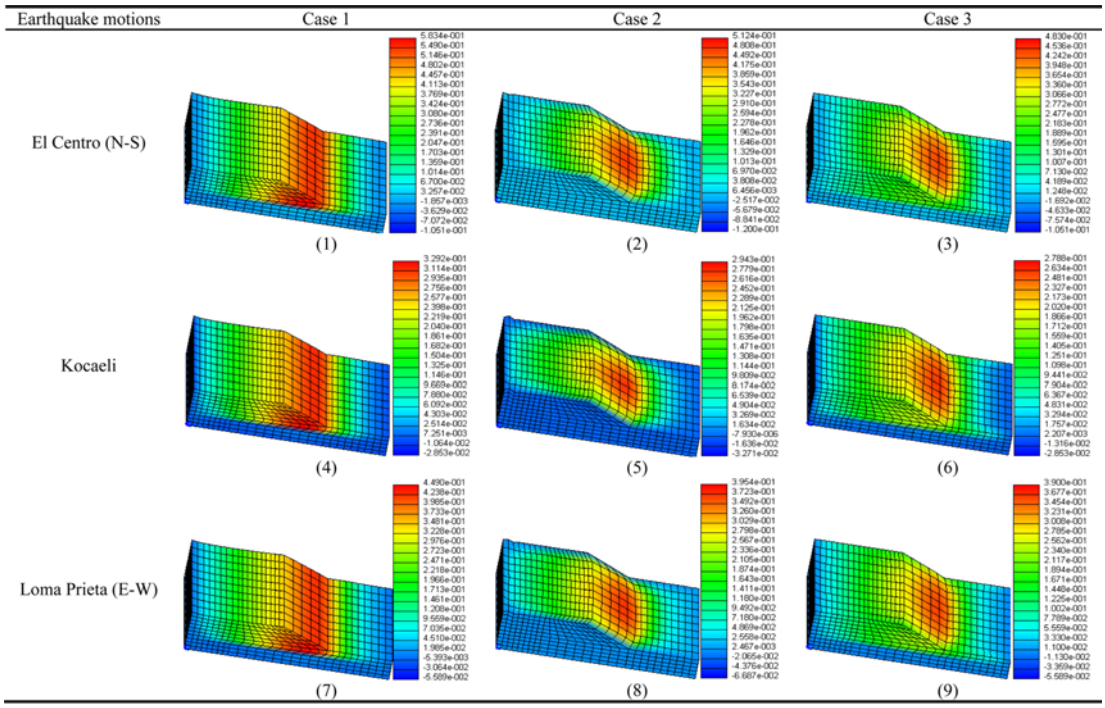

(c)

Fig. 6. (continued)

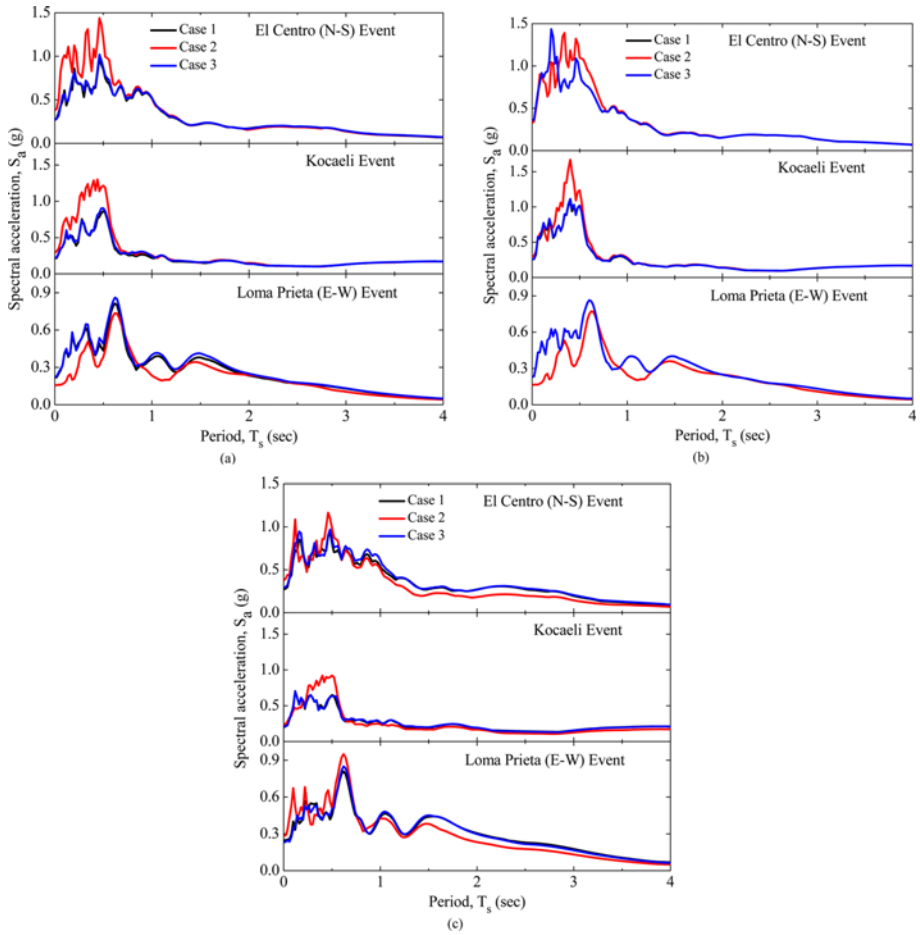

Fig. 7. Effect of Three-type Boundaries at Lateral Faces on the Acceleration Spectra at Node A: (a) Homogeneous Soil Slope, (b) Stratified Soil Slope, (c) Soil Slope with a Soft Clay Interlayer for α = 25°

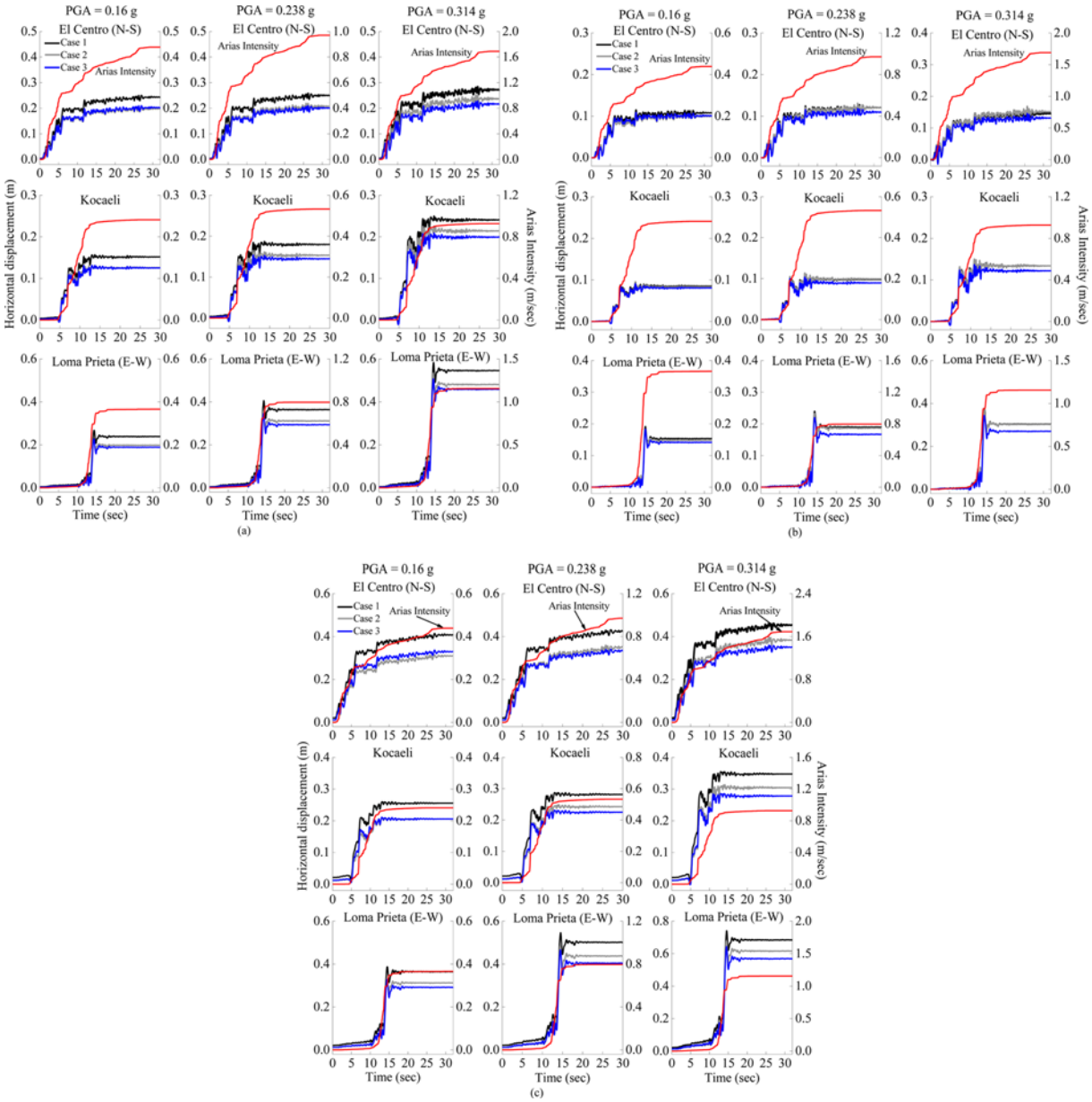

Fig. 8. Horizontal Displacement Time Histories at Node A for: (a) Homogeneous Soil Slope, (b) Stratified Soil Slope, (c) Soil Slope with a Soft Clay Interlayer for α = 25º

Table 3. First Ten Natural Frequencies of Cases 1-3 for Type 1 with Slope Angle of 25º

Mode number	Natural frequency (Hz)		
	Case 1 ($v = 0$)	Case 2 ($u = v = 0$)	Case 3 ($v = w = 0$)
1	0.534	0.547	0.535
2	0.643	0.65	0.645
3	0.661	0.679	0.662
4	0.711	0.723	0.715
5	0.762	0.779	0.763
6	0.789	0.802	0.794
7	0.798	0.805	0.800
8	0.828	0.843	0.830
9	0.838	0.851	0.844
10	0.842	0.877	0.865

Table 4. First Ten Natural Frequencies of Cases 1-3 for Type 2 with Slope Angle of 25º

Mode number	Natural frequency (Hz)		
	Case 1 ($v = 0$)	Case 2 ($u = v = 0$)	Case 3 ($v = w = 0$)
1	0.567	0.571	0.564
2	0.680	0.688	0.674
3	0.762	0.764	0.762
4	0.780	0.783	0.77
5	0.808	0.811	0.807
6	0.841	0.846	0.835
7	0.861	0.863	0.856
8	0.871	0.873	0.871
9	0.876	0.88	0.874
10	0.885	0.886	0.885

Table 5. First Ten Natural Frequencies of Cases 1-3 for Type 3 with Slope Angle of 25º.

Mode number	Natural frequency (Hz)		
	Case 1 ($v = 0$)	Case 2 ($u = v = 0$)	Case 3 ($v = w = 0$)
1	0.513	0.527	0.52
2	0.561	0.591	0.587
3	0.588	0.647	0.639
4	0.639	0.664	0.646
5	0.646	0.713	0.704
6	0.702	0.773	0.755
7	0.755	0.784	0.768
8	0.769	0.802	0.772
9	0.8	0.82	0.8
10	0.822	0.83	0.826

the types of soil slopes (Fig. 7). Additionally, the spectral accelerations at Node A in Case 2 are generally larger than the spectral accelerations at Node A in Cases 1 and 3 for the El Centro (N-S) and Kocaeli events. For the Loma Prieta (E-W) event, the spectral accelerations at Node A are similar in amplitude for Cases 1-3. The difference among the three boundaries is significant for the El Centro (N-S) and Kocaeli events compared to the Loma Prieta (E-W) event. The results are associated with the larger predominant period for the Loma Prieta (E-W) event (Table 2). Referring to Fig. 8, with PGA = 0.314 g, a significant difference is clearly observed among the three boundaries. For lower PGA, the difference in displacements at Node A between Case 2 and Case 3 decreases. Moreover, the differences among the three boundaries increase as the PGA in an event increases.

Hence, selecting an appropriate boundary of the lateral faces is important for a 3D slope seismic analysis. For a given large-scale 3D slope, fixing the displacement degrees of freedom only along the *y*-direction is not appropriate due to inaccurately predicting the seismic response of the slope and not considering the 3D effect. In addition, the PGA and predominant period in an earthquake event play important roles in the differences among the three boundaries at the lateral faces.

3.2 Influence of the Boundary Extent in the *y*-direction

To gauge the significance of the boundary extent along the *y*-direction, new meshes in Cases W_i, i = 1-7 (Fig. 9), for $\alpha = 25º$ are generated by increasing W relative to Mesh 1. For the given 3D soil slope, the minimum model width is 60 m in the Case W_1 (Fig. 9), the effect of the reflection of waves from the lateral boundaries ($y = 0$ and $y = 100$) is slight. Fig. 10 displays the influence of the W/H ($H = 15$ m) ratio on the permanent deformation at Nodes A, B, and C for the three types of soil slopes.

The permanent displacements at Nodes A, B, and C gradually increase with increasing W/H ratio ranging from 4 to 13.3. Under a specific W/H ratio ranging between 4 and 13.3, the ultimate permanent deformations at Nodes A, B, and C approach a constant value as W/H exceeds 12 for types 1 and 3. For type 2, when the W/H ratio exceeds 6, no appreciable effects are seen on the permanent deformation at Nodes A, B, and C (Fig. 10). It is also seen that a smaller W/H (width/height) ratio is obtained for stiffer soil, compared to soft soil, as the 3D effects induced by lateral boundaries become insignificant.

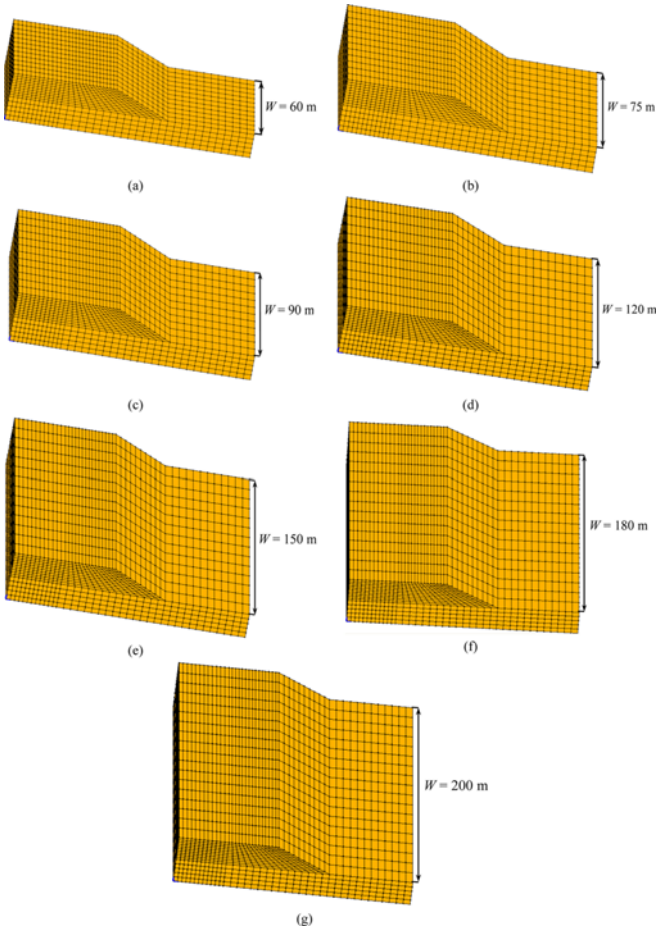

Fig. 9. Meshes with Changing Boundary Extent Along the *y*-direction: (a) Case W_1, (b) Case W_2, (c) Case W_3, (d) Case W_4, (e) Case W_5, (f) Case W_6, (g) Case W_7

In addition, when the W/H ratio exceeds the threshold values (i.e., 12 for types 1 and 3, 6 for type 2), the permanent deformation at Nodes A, B, and C is found to be approximately consistent with the corresponding results in Case 1. This result indicates that the 3D effect disappears, and the 2D deformation mechanism is formed with gradually increasing boundary extent in the *y*-direction.

4. Boundary Effect on the Seismic Response of Shallow Foundation on the Slope's Top

In this section, a set of numerical simulations are performed to explore the boundary effect on the seismic behaviors of shallow foundation on top of slopes. The soil slope for the numerical analysis is the same as before. The configuration and the meshes used for the shallow foundation founded near slope crests are presented in Fig. 11. Also, the homogeneous soil slope with a slope angle of 25º is used to show the FE meshes. As shown in

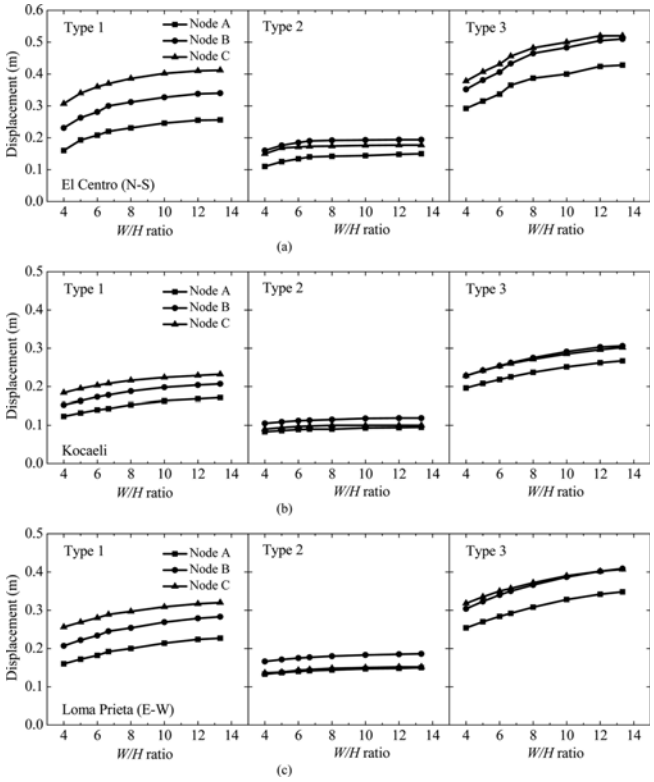

Fig. 10. Permanent Horizontal Displacement at Nodes A, B, and C for Various *W* Values for: (a) Homogeneous Soil Slope, (b) Stratified Soil Slope, (c) Soil Slope with a Soft Clay Interlayer for α = 25°

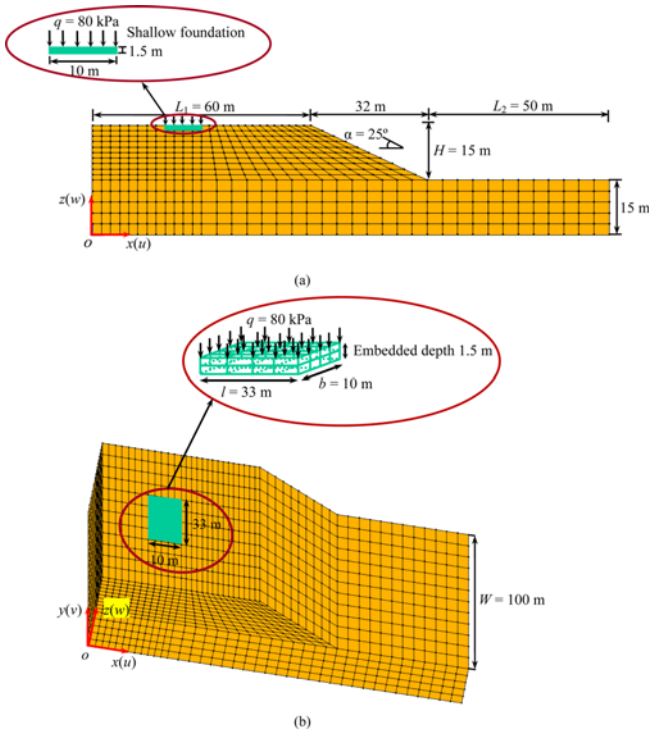

Fig. 11. Model Geometry and Finite Element Meshes for the Soil Slope-shallow Foundation System: (a) 2D Mesh, (b) 3D Mesh

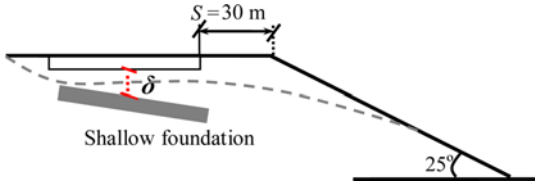

Fig. 12. An Illustration of the Seismic Settlement of Shallow Foundation

Fig. 11, a b = 10-m-wide and l = 33-m-long shallow foundation is considered and a pressure q = 80 kPa (representing an 8-story building on the shallow foundation) is applied on the surface of the foundation. Furthermore, the shallow foundation is embedded 1.5 m into the clay crust and the edge of the foundation is 30 m away from the slope crest (Fig. 11). The shallow foundation is modeled as a linear elastic material for simplicity (Karimi and Dashti, 2015) and is discretized into 8-node brick solid elements. The mass density of the foundation is 2500 kg/m^3 and its elastic modulus and Poisson ratio are 15 GPa and 0.2, respectively (Nour *et al*., 2002). The foundation elements are connected to the soil elements using equal degrees of freedom (Karimi and Dashti, 2015). In addition, the FE analysis is conducted in three consecutive steps: (i) application of own-weight of soil elements and the shallow foundation; (ii) application of surcharge load q onto the foundation; (iii) seismic shaking analysis in the time domain.

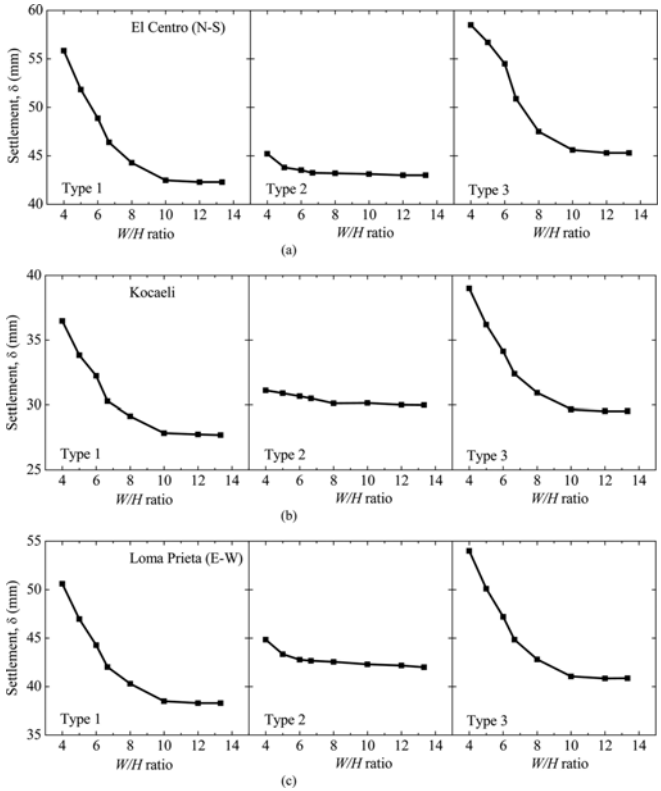

Fig. 13. Seismic Settlement of Shallow Foundation for: (a) Homogeneous Soil Slope, (b) Stratified Soil Slope, (c) Soil Slope with a Soft Clay Interlayer for α = 25°

The design of shallow foundations on top of slopes is generally controlled by the settlement. As a consequence, seismic settlement is a major concern and is an essential criterion in the design process of shallow foundations (Shahin *et al*., 2003). For ease of presentation, in Fig. 12 we plot an illustration of the seismic settlement (δ) of a shallow foundation. Fig. 13 displays the effect of W/H (H = 15 m) ratio on the settlement of the shallow foundation. As the lateral boundary of the slope is close to the shallow foundation (W/H = 4), a higher δ is observed (Fig. 13). Settlement is apparently decreased as the W/H ratio increases from 4 m to 10. When the W/H ratio increases even more (W/H = 12 or 13.3), the boundary extent effect disappears for types 1 and 3. However, for type 2, when the W/H ratio reaches/exceeds 6, no appreciable effects are seen on the settlement (Fig. 13).

In summary, for smaller W/H ratio (W/H = 4), the applied pressure onto the foundation becomes significant, in contrast to the smaller soil mass, large shear strain is mobilized under the foundation because of the applied pressure, so that greater settlement is obtained. Increasing the W/H ratio gives rise to a diversion of the deformation mechanism of the shallow foundation. That means, the foundation settlement that is controlled by the surcharge load and earthquake together before will be mostly affected by the seismic excitation.

5. Conclusions

A study is conducted to explore the boundary effects on the seismic response of a 3D slope and shallow foundation on the slope's top. Some important results are:

1. In the seismic analysis of the given 3D slope, fixing the displacement degrees of freedom only in the y-direction (perpendicular to the shaking direction) at the lateral boundaries is inappropriate, because this boundary cannot exhibit the 3D effect.
2. For the given 3D slope, a 2D analysis is appropriate if the width/height ratio (W/H) of the slope is greater than 12 for geometry types 1 and 3, and greater than 6 for geometry type 2.
3. An increase in the peak ground accelerations of earthquake events tends to enlarge the difference among the three lateral boundaries. On the other hand, for an earthquake event with a larger predominant period, the differences between the three lateral boundaries are small.
4. For the given shallow foundation on top of slopes, the foundation settlement, that is controlled by the applied pressure and earthquake loading together, will be mostly affected by the seismic excitation, when the boundary extent along the y-direction is increased.
5. Overall, the conducted study highlights the boundary effects on the earthquake performances of a 3D soil slope with a shallow foundation on top, and provides insight for engineers in the process of choosing an appropriate boundary in a numerical analysis. The influence of boundary conditions on the seismic stability and on the critical slip surface of the soil slope will be addressed in future studies.

Acknowledgements

We gratefully acknowledge support for this research from the State Key Program of National Natural Science of China (Grant No. 41430634), the National Natural Science Foundation of China (Grant Nos. 51578195, 51378161, and 51308547), the Opening Fund for Innovation Platform of China (Grant No. 2016YJ004), and the Technology Research and Development Plan Program of China railway corporation (Grant No. 2016G002-F). Professor Andrew Chan at the University of Tasmania provided useful suggestions for improving the manuscript.

Notations

α = Slope angle
b = Width of shallow foundation
B = Bulk modulus of soil skeleton
f_m = Yield surface, m = 1, 2, ..., NYS
G_r = The low-strain shear modulus
H = Slope height
H_m = Elastoplastic (tangent) shear modulus, m = 1, 2, ..., NYS
H_{NYS} = Elastoplastic (tangent) shear modulus when the number of yield surfaces equals to NYS
l = Length of shallow foundation
M_f = The size of yield surface when the shear stress reaches the ultimate shear strength
M_m = The size of yield surface, m = 1, 2, ..., NYS
M_{NYS} = The size of yield surface when the number of yield surfaces equals to NYS
NYS = The total number of yield surfaces
p'_r = Reference confinement
p'_0 = Initial confinement
q = Surcharge load
u = The displacement degrees of freedom in the x-direction
v = The displacement degrees of freedom in the y-direction
w = The displacement degrees of freedom in the z-direction
W_i = Slope meshes (i = 1-7)
W = Slope width in the y-direction
W/H = The ratio of slope width to slope height
δ = The seismic settlement of shallow foundation
η = Poisson ratio
τ = The octahedral shear stress
τ_f = The ultimate shear strength
τ_{max} = The maximum shear strength
τ_{m+1} = The shear strength when the number of yield surfaces equals to m+1, m = 1, 2, ..., NYS
τ_m = The shear strength when the number of yield surfaces equals to m, m = 1, 2, ..., NYS
τ_{NYS} = The maximum shear strength when the number of yield surfaces equals to NYS
γ = The octahedral shear strain
γ_r = γ approaches ∞
γ_{max} = The maximum shear strain
γ_{m+1} = The shear strain when the number of yield surfaces

equals to m+1, m = 1, 2, ..., NYS

γ_m = The shear strain when the number of yield surfaces equals to m, m = 1, 2, ..., NYS

References

Azizian, A. and Popescu, R. (2006). "Three-Dimensional seismic analysis of submarine slopes." *Soil Dynamics and Earthquake Engineering*, Vol. 26, No. 9, pp. 870-887, DOI: 10.1016/j.soildyn.2005.10.008.

Azzam, W. R. (2015). "Finite element analysis of skirted foundation adjacent to sand slope under earthquake loading." *HBRC Journal*, Vol. 11, No. 2, pp. 231-239, DOI: 10.1016/j.hbrcj.2014.04.001.

Bienen, B., Gaudin, C., and Cassidy, M. J. (2007). "Centrifuge tests of shallow footing behaviour on sand under combined vertical-torsional loading." *International Journal of Physical Modelling in Geotechnics*, Vol. 7, No. 2, pp. 1-21, DOI: 10.1680/ijpmg.2007.070201.

Bouckovalas, G. D. and Papadimitriou, A. G. (2005). "Numerical evaluation of slope topography effects on seismic ground motion." *Soil Dynamics and Earthquake Engineering*, Vol. 25, No. 7, pp. 547-558, DOI: 10.1016/j.soildyn.2004.11.008.

Choudhury, D. and Subba Rao, K. S. (2006). "Seismic bearing capacity of shallow strip footings embedded in slope." *International Journal of Geomechanics*, Vol. 6, No. 3, pp. 176-184, DOI: 10.1061/(ASCE) 1532-3641(2006)6:3(176).

Deng, L. and Kutter, B. L. (2012). "Characterization of rocking shallow foundations using centrifuge model tests." *Earthquake Engineering and Structural Dynamics*, 2012; Vol. 41, No. 5, pp. 1043-1060, DOI: 10.1002/eqe.1181.

Drosos, V., Georgarakos, T., Loli, M., Anastasopoulo, I., Zarzouras, O., and Gazetas, G. (2012). "Soil-foundation-structure interaction with mobilization of bearing capacity: Experimental study on sand." *Journal of Geotechnical and Geoenvironmental Engineering*, Vol. 138, No. 11, pp. 1369-1386, DOI: 10.1061/(ASCE)GT.1943-5606.0000705.

Gajan, S., Kutter, B. L., Phalen, J. D., Hutchinson, T. C., and Martin, G. R. (2005). "Centrifuge modeling of load-deformation behavior of rocking shallow foundations." *Soil Dynamics and Earthquake Engineering*, Vol. 25, No. 7, pp. 773-783, DOI: 10.1016/j.soildyn. 2004.11.019.

Gajan, S. and Kutter, B. L. (2009). "Effects of moment-to-shear ratio on combined cyclic load-displacement behavior of shallow foundations from centrifuge experiments." *Journal of Geotechnical and Geoenvironmental Engineering*, Vol. 135, No. 8, pp. 1044-1055, DOI: 10.1061/(ASCE)GT.1943-5606.0000034.

Iwan, W. D. (1976). "On a class of models for the yielding behavior of continuous and composite systems." *Journal of Applied Mechanics*, Vol. 34, No. 3, pp. 612-617, DOI: 10.1115/1.3607751.

Karimi, Z. and Dashti, S. (2015). "Numerical and centrifuge modeling of seismic soil-foundation-structure interaction on liquefiable ground." *Journal of Geotechnical and Geoenvironmental Engineering,* Vol. 142, No. 1, pp. 04015061, DOI: 10.1061/(ASCE)GT.1943-5606.0001346.

Kourkoulis, R., Anastasopoulos, I., Gelagoti, F., and Gazetas, G. (2010). "Interaction of foundation-structure systems with seismically precarious slopes: Numerical analysis with strain softening constitutive model." *Soil Dynamics and Earthquake Engineering*, Vol. 30, No. 12, pp. 1430-1445, DOI: 10.1016/j.soildyn.2010.05.001.

Liu, S. Y., Shao, L. T., and Li, H. J. (2015). "Slope stability analysis using the limit equilibrium method and two finite element methods." *Computers and Geotechnics*, Vol. 63, pp. 291-298, DOI: 10.1016/ j.compgeo.2014.10.008.

Lu, J., Yang, Z., and Elgamal, A. (2010). *OpenSeesPL 3D lateral pile-ground interaction: User manual*. University of California, San Diego, USA.

Maugeri, M., Musumeci, G., Novità, D., and Taylor, C. A. (2000). "Shaking table test of failure of a shallow foundation subjected to an eccentric load." *Soil Dynamics and Earthquake Engineering*, Vol. 20, No. 5, pp. 435-444, DOI: 10.1016/S0267-7261(00)00091-9.

Mazzoni, S., McKenna, F., Scott, M. H., and Fenves, G. L. (2009). *Open system for earthquake engineering simulation user manual*, University of California, Berkeley, California, <http://opensees.berkeley.edu/>.

Mroz, Z. (1967). "On the description of anisotropic work hardening." *Journal of the Mechanics and Physics of Solids*, Vol. 15, No. 3, pp. 163-175, DOI: 10.1016/0022-5096(67)90030-0.

Nour, A., Slimani, A., and Laouami, N. (2002). "Foundation settlement statistics via finite element analysis." *Computers and Geotechnics*, Vol. 29, No. 8, pp. 641-672, DOI: 10.1016/S0266-352X(02)00014-9.

Paolucci, R., Shirato, M., and Yilmaz, M. T. (2008). "Seismic behaviour of shallow foundations: Shaking table experiments vs numerical modelling." *Earthquake Engineering and Structural Dynamics*, Vol. 37, No. 4, pp. 577-595, DOI: 10.1002/eqe.773.

Parra, E. (1996). *Numerical modeling of liquefaction and lateral ground deformation including cyclic mobility and dilation response in soil systems*, PhD Thesis, Rensselaer Polytechnic Institute, Troy, N. Y.

Raychowdhury, P. and Hutchinson, T. C. (2009). "Performance evaluation of a nonlinear Winkler-based shallow foundation model using centrifuge test results." *Earthquake Engineering and Structural Dynamics*, Vol. 38, No. 5, pp. 679-698, DOI: 10.1002/eqe.902.

Shahin, M. A., Maier, H. R., and Jaksa, M. B. (2003). "Settlement prediction of shallow foundations on granular soils using B-spline neurofuzzy models." *Computers and Geotechnics*, Vol. 30, No. 8, pp. 637-647, DOI: 10.1016/j.compgeo.2003.09.004.

Shirato, M., Kouno, T., Asai, R., Nakatani, S., Fukui, J., and Paolucci, R. (2008). "Large-scale experiments on nonlinear behavior of shallow foundations subjected to strong earthquakes." *Soils and Foundations*, Vol. 48, No. 5, pp. 673-692, DOI: 10.3208/sandf.48.673.

Taiebat, M., Kaynia, A. M., and Dafalias, Y. F. (2011). "Application of an anisotropic constitutive model for structured clay to seismic slope stability." *Journal of Geotechnical and Geoenvironmental Engineering,* Vol. 137, No. 5, pp. 492-504, DOI: 10.1061/(ASCE)GT.1943-5606.0000458.

Tripe, R., Kontoe, S., and Wong, T. K. C. (2013). "Slope topography effects on ground motion in the presence of deep soil layers." *Soil Dynamics and Earthquake Engineering*, Vol. 50, No. 7, pp. 72-84, DOI: 10.1016/j.soildyn.2013.02.011.

Trombetta, N. W., Mason, H. B., Chen, Z., Hutchinson, T. C., Bray, J. D., and Kutter, B. L. (2013). "Nonlinear dynamic foundation and frame structure response observed in geotechnical centrifuge experiments." *Soil Dynamics and Earthquake Engineering*, Vol. 50, pp. 117-133, DOI: 10.1016/j.soildyn.2013.02.010.

Yang, Z., Elgamal, A., and Parra, E. (2003). "Computational model for cyclic mobility and associated shear deformation." *Journal of Geotechnical and Geoenvironmental Engineering*, Vol. 129, No. 12, pp. 1119-1127, DOI: 10.1061/(ASCE)1090-0241(2003)129:12(1119).